Excited-state dynamics of o-nitrophenol studied with UV pump–VUV probe time-resolved photoelectron and photoion spectroscopy

McClung et al.

Samuel McClung; Dakshitha Abeygunewardane; Spiridoula Matsika; ... et. al



J. Chem. Phys. 158, 144303 (2023) https://doi.org/10.1063/5.0146399





CrossMark

Articles You May Be Interested In

OH produced from o -nitrophenol photolysis: A combined experimental and theoretical investigation

J. Chem. Phys. (June 2009)

Studies on novel co-crystal of 2, 6-diaminopyridinium 4-nitrophenolate 4-nitrophenol.

AIP Conference Proceedings (June 2012)

Crystal growth and characterization of 4-dimethylamino pyridinium 4-nitrophenolate 4-nitrophenol (DMAPNP) for NLO applications

AIP Conference Proceedings (July 2019)





.Downloaded from http://pubs.aip.org/aip/jcp/article-pdf/doi/10.1063/5.0146399/16825313/144303_1_5.0146399.pd



Excited-state dynamics of o-nitrophenol studied with UV pump-VUV probe time-resolved photoelectron and photoion spectroscopy

Cite as: J. Chem. Phys. 158, 144303 (2023); doi: 10.1063/5.0146399 Submitted: 13 February 2023 • Accepted: 27 March 2023 •









Published Online: 13 April 2023

Samuel McClung, Dakshitha Abeygunewardane, DSpiridoula Matsika, Dand Thomas Weinacht D







AFFILIATIONS

- Department of Physics and Astronomy, Stony Brook University, Stony Brook, New York 11794, USA
- Department of Chemistry, Temple University, Philadelphia, Pennsylvania 19122, USA
- a) Author to whom correspondence should be addressed: thomas.weinacht@stonybrook.edu

ABSTRACT

Time-resolved photoionization measurements were performed on o-nitrophenol pumped with UV laser pulses at a central wavelength of 255 nm (4.9 eV) and probed with vacuum ultraviolet (VUV) pulses at 153 nm (8.1 eV). The photoelectron spectrum and time of flight mass spectrum for ions were recorded at each pump-probe delay. The measurements are interpreted with the aid of electronic structure calculations for both the neutral and ionic states. Evidence is found for the formation of a bicyclic intermediate followed by NO dissociation through a process of internal conversion and intersystem crossing. The combination of photoelectron and photoion spectroscopy, together with computational results, provides strong evidence of intersystem crossing that is difficult to establish with only a single technique.

Published under an exclusive license by AIP Publishing. https://doi.org/10.1063/5.0146399

I. INTRODUCTION

The excited-state dynamics of photoexcited molecules determine the outcome of many natural processes such as photosynthetic light harvesting¹ and DNA photoprotection²⁻⁴ and have potential technological applications for solar energy conversion⁵ and optoelectronics.⁶ Time-resolved photoelectron spectroscopy (TRPES) allows one to track the flow of energy in excited molecular systems, although it provides limited information on time evolving structures. Diffractive measurements allow one directly to probe time dependent structures, but they usually involve larger scale facilities.^{8–11} Photoion spectroscopy experiments can also provide information on structural changes, if they are performed with momentum resolution of the fragment ions and/or performed in conjunction with structure or dynamics calculations that allow for detailed interpretation of the fragment ion yields.¹

Interactions between o-nitrophenol and solar UV have been studied extensively, with particular emphasis on HONO dissociation since the HONO molecules can lead to the formation of smog.¹³ Previous ultrafast experimental and theoretical studies on o-nitrophenol have shown a broad range of dynamics, including internal conversion (IC), intersystem crossing (ISC), excited-state intramolecular proton transfer (ESIPT), and HONO

dissociation. 14-19 A majority of these studies explored photodynamics following electronic excitation to the first excited singlet state (S_1) with photon energies around 3.6 eV. The results of resonance Raman spectroscopy, 14 time-resolved photoelectron spectroscopy coupled with density functional theory (DFT) calculations, 15 reference ab initio theoretical calculations, 17 and non-adiabatic molecular dynamics simulations^{18,19} provide a picture of relaxation following excitation to S₁: ultrafast intersystem crossing to T₂ or T₁ (due to strong spin orbit coupling), ESIPT occurring predominantly on T₁, and subsequent HONO dissociation on T₁, or the formation of a vibrationally hot ground state after internal conversion to S_0 . The theoretical kinetic barriers for the formation of various products on the S₁ and T₁ surfaces have been reported, with the lowest barrier observed for the formation of nitrosophenoxy + OH through the aci-o-nitrophenol intermediate. The same study also hypothesizes a fragmentation channel that forms hydroxyphenoxy + NO via a spiro-bicyclic nitro-nitrite intermediate but notes that it is relevant when more energy is available to the molecule and competes with other channels.²⁰ Experimental studies of dynamics from higher lying bright excited states, such as S₄, have been limited.²

In this work, the excited-state dynamics of o-nitrophenol are studied after excitation at 255 nm (4.9 eV). We use a combination of time-resolved ion spectroscopy (TRIS) and time-resolved photoelectron spectroscopy (TRPES) and make use of the electronic structure calculations to determine the electronic states involved and the dissociation pathways leading to the observed fragments.

II. COMPUTATIONAL DETAILS

All geometry optimizations were performed using the complete active space self-consistent field (CASSCF) method, with an active space consisting of 12 electrons in 10 orbitals (HOMO-6 to HOMO+3) and the 6-311+G(d) basis set [CASSCF(12, 10)/6-311+G(d)]. Energies of excited states were calculated with state averaged CASSCF, averaging over seven singlet and five triplet states using equal weights [12SA-CASSCF(12, 10)/6-311+G(d)] for all geometries mentioned in this work. The CASSCF energies were corrected with the single state, single reference, complete active space second order perturbation theory (CASPT2), containing six singlet and four triplet states. Energies of the ionic states and Dyson norms between the neutral excited states and the ionic states were calculated using equation of motion-coupled cluster with singles and doubles for ionization potentials (EOM-IP-CCSD) with the 6-311+G(d) basis set. Ionization potential (IP) for possible fragments of nitrophenol (HONO and hydroxyphenoxy) were calculated at the EOM-IP-CCSD/6-311+G(d) level using the ground state minima optimized by density functional theory, specifically B3LYP/6-311+G(d).

A pathway connecting the initial Franck-Condon (FC) geometry to the observed products was created. The hypothesized reaction coordinate consists of three main structures: the ground state minimum o-nitrophenol (S₀-NP), the intermediate prior to NO dissociation (Spiro-NP), and the fragments following NO dissociation (hydroxyphenoxy and NO). The structure of Spiro-NP was obtained by geometry optimization along the first excited triplet state (T₁) surface, starting from a structure resembling the intermediate proposed by Vereecken et al.20 A subsequent vibrational frequency calculation resulted in all positive frequencies, which leads to the conclusion that Spiro-NP represents a local minimum on the T₁ surface. The points between S₀-NP and Spiro-NP were obtained by linear interpolation of internal coordinates (LIIC). They were further refined using constrained optimization restricting the C-O bond using 12SA-CASSCF(12, 10)/6-311+G(d). Optimizations were done along both the S₁ and T₁ surfaces in order to determine the barrier for each state. The points between Spiro-NP and the dissociated fragments were obtained with constrained optimization along T₁ using CASSCF, where the length of the C-N bond was constrained. Excited-state energies along the path were calculated at higher accuracy using single point CASPT2(12, 10)/6-311+G(d) calculations, as well as equation of motion-coupled cluster with singles and doubles for excitation energies (EOM-EE-CCSD) with 6-311+G(d). Constrained optimizations restricting the C-O bond were also done for the cation ground state D₀ using EOM-IP-CCSD/6-311+G(d) in order to obtain a barrier for dissociation for the cation.

The CASSCF and CCSD calculations were performed with Molpro (2021.1) and Q-Chem (5.4.1), respectively.

III. EXPERIMENTAL SETUP

Experiments were performed using a titanium sapphire laser system, which produced 1 mJ pulses centered at 775 nm with a

repetition rate of 1 KHz. Pump pulses were produced via thirdharmonic generation (255 nm, 4.9 eV), and probe pulses were produced from fifth-harmonic generation (153 nm, 8.1 eV) via noncollinear four-wave mixing in an argon cell.²² The detector consisted of three velocity-map imaging (VMI) plates, two microchannel plates (MCPs) to amplify the signal, a phosphor screen that can map hit positions in 2D via fluorescence, and a CMOS camera to image the phosphor screen. Ion yields were measured using a digital oscilloscope to record the voltage from the hits on the detector. The time of flight (ToF) of the hits allowed for discrimination between the parent and fragment ion yields. For electrons, we recorded the two-dimensional projection of the full 3D momentum distribution. Utilizing the 2D momentum information from the phosphor images and the cylindrical symmetry about the polarization axis (ppolarization in the plane of the detector for both the pump and probe pulses), inverse Abel transforms were calculated to determine the full 3D momentum, and thereby the energy distribution of the electrons as a function of time delay. The pump-probe time zero was determined by performing a pump-probe measurement with ethylene. Ethylene was also used to calibrate the time resolution, by modeling the ethylene signal as a convolution of the "true" signal (the rapid exponential decay of the ethylene yield), ^{23–25} and a Gaussian instrument response function (IRF). The time resolution was measured to be about 90 fs, using the FWHM of the IRF as a metric. Powder samples of o-nitrophenol (Sigma-Aldrich, 98% purity) were used to produce an effusive beam in the VMI chamber through a thin nozzle.

IV. RESULTS/DISCUSSION

Ion ToF traces show yields of parent ion and multiple fragments. However, after subtracting a background trace at a pump–probe delay of –500 fs, the two prominent peaks showing delay-dependent yields were masses 139 and 109 amu, as shown in Fig. 1. These peaks correspond, respectively, to the parent ion and a hydroxyphenoxy fragment that forms from NO dissociation.²⁰ Previous work on the excited-state dynamics of nitrophenol showed evidence of HONO dissociation after isomerization, ^{13,15} but there

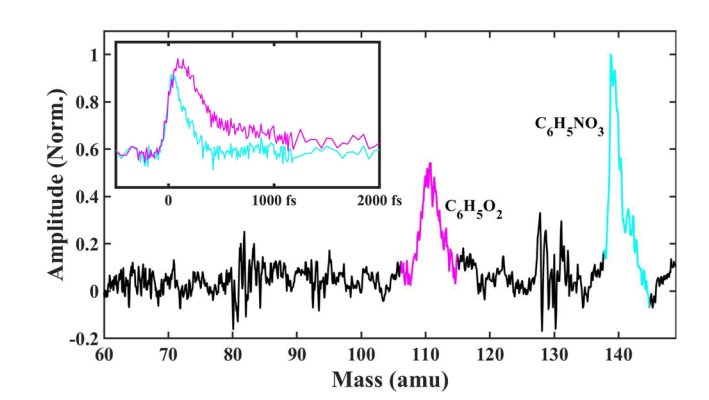


FIG. 1. ToF trace at delay = 30 fs. A "background" ToF trace at delay = -500 fs was subtracted from the trace at 30 fs to produce the result shown. The inset shows the time-dependent integrated parent ion yield (cyan) and hydroxyphenoxy ion yield (magenta), with the integration regions color-coded in the ToF trace.

has not been any previous observation of neutral photodissociation to form NO and hydroxyphenoxy. A pathway for this dissociation, however, which requires the rearrangement of the NO_2 group, has been shown theoretically for the ground singlet and lowest triplet surfaces. ²⁰

Motivated by the intermediate proposed by Vereecken *et al.*, ²⁰ calculations were performed to determine how the hydroxyphenoxy fragment is formed upon excitation of nitrophenol at 255 nm. The calculation results are summarized in Fig. 2. Excitation at 255 nm (4.84 eV) launches a wave packet on the S₄ state, which can undergo rapid internal conversion to lower electronic states, as well as intersystem crossing to triplet states. The lowest triplet state is particularly interesting because there is a low barrier to isomerization (forming Spiro-NP) and dissociation (forming hydroxyphenoxy + NO). This motivates TRPES to follow the internal conversion dynamics (via changes to the photoelectron energies as a function of pump–probe delay) and TRIS to follow the isomerization and dissociation dynamics (via changes to the fragment ion yields vs pump–probe delay).

The TRPES experiments reveal excitation to the S_4 state followed by ionization to the D_0 and D_1 states, as shown in Fig. 3. Ionization to these states is predicted based on the Dyson norms, which are proportional to the probability for one photon ionization. The Dyson norms are calculated to be 0.29 and 0.60, for D_0 and D_1 states, respectively. The S_4 state is described as a pi -> pi* excitation, and the most likely ionization event is removing an electron from pi* leading to D_1 , justifying the large Dyson norm. Some ionization to D_0 occurs as well because of configuration mixing. The photoelectron spectrum at zero time delay shows a large peak from 1.5 to 3 eV, consistent with ionization to D_1 , as well as some yield between 3 and 4 eV, consistent with ionization to D_0 facilitated by configuration mixing. The electron yield and

average energy exhibit rapid decays, consistent with rapid internal conversion to S_1 .

With regard to the ion data, the clear visibility of the 139 and 109 amu peaks after background subtraction indicates significant time dependence in the yields and branching ratio. The time dynamics were further investigated by integrating the yields from the two peaks at each time delay. The results of this integration are shown in the inset of Fig. 1 and in more detail in Fig. 4. The yield curves are both normalized with respect to the maximum parent ion yield, which means the hydroxyphenoxy ion yield has a slightly larger maximum amplitude. The time at which the hydroxyphenoxy ion yield is maximum differs from the parent ion by about 50 fs, suggesting a transformation enhancing the hydroxyphenoxy yield which takes about 50 fs.

In order to quantify the differences between the parent and hydroxyphenoxy yields, the yields are fit to a model which considers exponential decay of both yields, with both prompt and delayed contributions to the hydroxyphenoxy ion yield. The delay between the parent and hydroxyphenoxy yields motivates the delayed contribution in the model, while the fact that the hydroxyphenoxy yield is larger than the parent, and that it also appears in electron impact spectra, ²⁶ motivates a prompt contribution (i.e., vertical ionization followed by dissociation of the cation) in the model.

The parent ion data are fit to an exponential decay,

$$N_{parent}(t) = \theta(t_0) N_{parent}(t_0) e^{-(t-t_0)/\tau_1},$$
 (1)

convolved with the Gaussian IRF. Here, $\theta(t)$ represents a Heaviside step function. From the fit, the decay constant is found to be $\tau_1 = 118 \pm 13$ fs. The hydroxyphenoxy fragment ion yield is modeled as coming from a combination of two different mechanisms

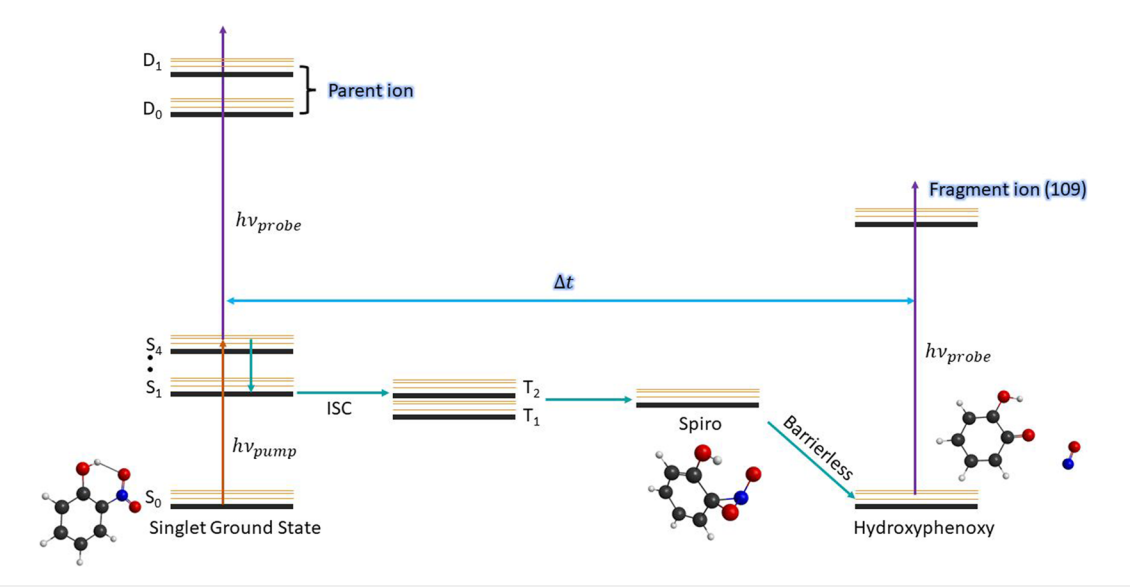


FIG. 2. Illustration of the proposed dynamics. The o-nitrophenol molecule is excited to the S_4 state and can be ionized from this state with the probe photon. The molecule undergoes internal conversion to the S_1 state and intersystem crossing to triplet states. From the T_1 state, the o-nitrophenol forms an intermediate spiro-bicyclic structure and then dissociates to form hydroxyphenoxy and NO.

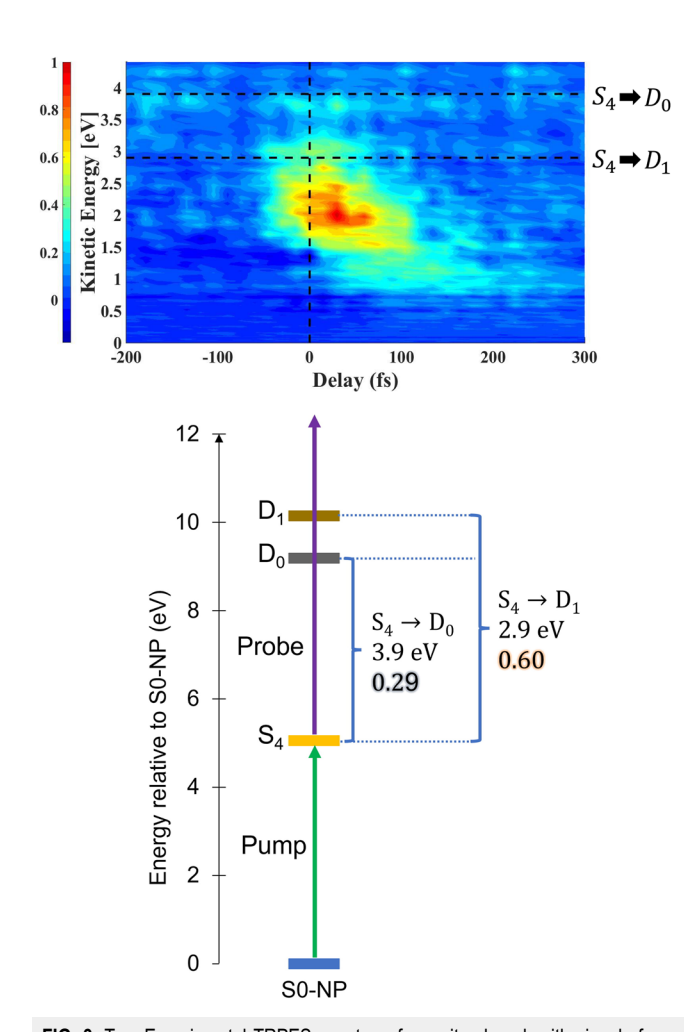


FIG. 3. Top: Experimental TRPES spectrum for o-nitrophenol, with signals from ionic states D_0 and D_1 labeled. Bottom: The energies of these states and Dyson norms of ionization from the S_4 state. Excitation energies of neutral nitrophenol are calculated at the CASPT2 level, while ionization energies and Dyson norms are calculated at the EOM-IP-CCSD level. Dyson norms are indicated with bold gray and brown colors for the S_4 -D $_0$ and S_4 -D $_1$ pairs, respectively.

(with yields labeled $N_{fragment,1}$ and $N_{fragment,2}$) plus a constant C that could be interpreted as a "long-term" decay process beyond the time scale investigated. Here, $N_{fragment,1}$ and $N_{fragment,2}$ represent (1) fragment ions produced directly by the pump and probe pulses without intervening molecular dynamics and (2) a separate, sequential process that involves some excited-state dynamics between the pump and probe pulses. A model containing only the sequential mechanism was found to be incomplete in capturing the dynamics of the fragment ion yield, as shown in Appendix A. Accounting for the two mechanisms, the full yield becomes

$$N_{fragment} = \theta(t_0)(\alpha N_{fragment,1} + \beta N_{fragment,2} + C),$$
 (2)

in which α and β are coefficients of proportionality such that $\alpha + \beta = 1$. The equations for the two components are then

$$N_{fragment,1}(t) = N_{fragment}(t_0)e^{-(t-t_0)/\tau_2},$$
 (3)

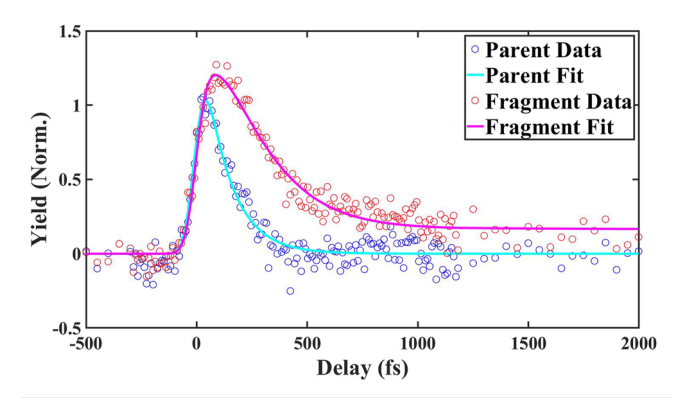


FIG. 4. Parent and hydroxyphenoxy fragment ion yields as a function of pump–probe delay together with fits to the data. The data and fits are normalized with respect to the maximum parent ion yield.

$$N_{fragment,2}(t) = N_{fragment}(t_0)e^{-(t-t_0)/\tau_2} + \frac{\tau_2}{\tau_1 - \tau_2}N_{parent}(t_0)(e^{-(t-t_0)/\tau_1} - e^{-(t-t_0)/\tau_2}).$$
(4)

The combination of these equations, as described above, results in the equation

$$N_{fragment}(t) = \theta(t_0) \left(N_{fragment}(t_0) e^{-(t-t_0)/\tau_2} + \frac{\beta \tau_2}{\tau_1 - \tau_2} N_{parent}(t_0) (e^{-(t-t_0)/\tau_1} - e^{-(t-t_0)/\tau_2}) + C \right).$$
(5)

Fitting the fragment data to this equation, with the results from the parent ion fit, the fragment fit parameters are found to be $\tau_2 = 190 \pm 30$ fs, $\beta = 0.7 \pm 0.4$, and $C = 0.164 \pm 0.009$. Although the fit allows a value of $\beta = 1.1$ within the uncertainty, only values of β between zero and one make physical sense. The fitting results suggest that most of the hydroxyphenoxy ion yield ($\beta = 0.7$) is produced by ionization of the molecule from an intermediate structure (i.e., Spiro) formed on the excited state in about 118 fs (τ_1), with dissociation to form hydroxyphenoxy taking place in about another 190 fs (τ_2). The fact that the fits produce a nonzero value for the long time yield of the hydroxyphenoxy ion (C = 0.164), whose ionization potential of 8.1 eV allows for some threshold ionization by the probe pulse, is consistent with neutral dissociation. These ion results are compared to the electron data in Appendix C.

A more detailed description of the pathway from the parent molecule to the spiro-intermediate and then to the hydroxyphenoxy + NO dissociation is shown in Fig. 5. There are two parts to this pathway; the first one connects the initial Franck–Condon structure to the Spiro intermediate via linearly interpolated geometries, while the second part is obtained from a constrained optimization along the T_1 surface with the dissociating C–N coordinate constrained. These calculations show that the initially populated S_4 state can rapidly decay to the lowest S_1 state because of the high density of states. Based on previous theoretical and experimental calculations, we expect that intersystem crossing from S_1 to the triplet manifold

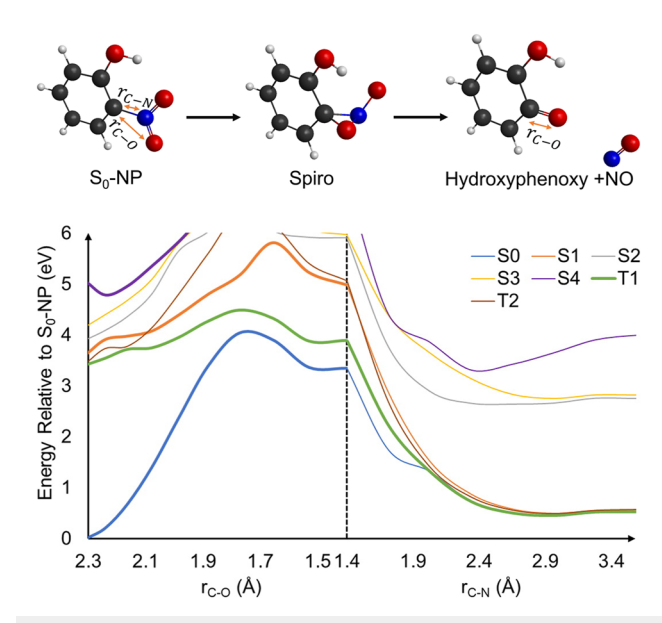


FIG. 5. Energies at the CASPT2/6-311+G(d) level of five singlet and two triplet electronic states of nitrophenol along the proposed reaction pathway to HPN + NO. In the first half, interpolated geometries (LIICs) from S_0 -NP to Spiro-NP are used, while the geometries of the second half are obtained from constrained optimizations along NC.

will be very fast. ^{16–18} Specifically, surface hopping calculations predicted the intersystem crossing to happen in less than 100 fs, ¹⁸ while previous photoelectron spectra supported these fast timescales. ¹⁶

The most important observation from Fig. 5 is that the T_1 state is the only state that does not have a significant energy barrier along this reaction pathway, unlike the S₁ state, which has a large barrier. It should be noted that the barriers shown in this figure are not the true barriers but rather upper estimates of the true barriers. An additional plot of this path is shown in Fig. 7 using EOM-EE-CCSD, which also confirms that T₁ is the reactive state for dissociation. The true barriers have been calculated using the constrained optimizations along S_1 and T_1 , and it was confirmed that the barrier on T_1 is about 0.5-0.6 eV, while that on S₁ is 1.7-1.8 eV (using electronic structure theory that includes correlation, CASPT2, and CCSD). Table I shows the barriers using different levels of theory. The low barrier on the T₁ state is further evidence that intersystem crossing is necessary in the formation of hydroxyphenoxy + NO, making this fragment a clear signature of intersystem crossing. Based on these energies, we can also explain why the hydroxyphenoxy + NO pathway has not been detected when exciting to S₁, since this does not provide enough energy to overcome the barrier on T_1 , which, although small, is not negligible. On the other hand, excitation to S₄ provides the extra energy that can easily be used to go over the barrier and reach the Spiro intermediate. Once the intermediate is reached, further dissociation is spontaneous, as indicated on the right side of Fig. 5.

In order to investigate whether dissociation can happen directly in the cation, we calculated the energies of low lying states of the molecular cation as a function of C–O bond length, i.e., from the S_0 minimum to the Spiro intermediate. The strict LIIC geometries

TABLE I. Barriers (in eV) connecting S_0 -NP to Spiro-NP along the minimum energy paths on S_1 and T_1 surfaces obtained by constrained optimizations along the C–O bond. Geometries were generated using 12SA-CASSCF(12, 10) and gradients for the respective state.

	CASSCF	CCSD	CASPT2
$\overline{S_1}$	1.60	1.83	1.71
T_1	1.33	0.56	0.46

were used, as well as geometries generated by constrained optimization along D_0 . The calculations, whose results are shown in Fig. 7, indicate that both D₀ and D₁, which have sizable Dyson norms from the excited states, have barriers to dissociation and do not facilitate the production of the hydroxyphenoxy fragment ion. The barrier on D₀ based on the constrained optimization calculations is found to be 1.27 eV. We note, however, that these results also provide a mechanism for the formation of the hydroxyphenoxy fragment ion via vertical ionization from the ground state with energies above 11 eV. The vertical ionization energy of D₂ is less than the combined pump and probe pulse energies (13 eV). Ionization to D₂ provides the molecule with sufficient energy to lead to dissociation, by internal conversion to the lower cationic states, which has been found to take place on femtosecond timescales.²⁸ The conversion of electronic energy into vibrational on D₀ provides enough energy to overcome the barrier to dissociation. In conclusion, non-resonant ionization from the ground state of the neutral molecule with pump + probe (13 eV) can produce D₀, D₁, and D₂. While D₀ and D₁ cannot fragment, D₂ can (via internal conversion), producing some fragment ions for zero pump-probe delay. However, following excitation by the pump pulse, Dyson norms for ionization by the probe pulse favor only D₀ and D₁, which do not fragment if created near the ground state minimum geometry. Thus, while fragmentation in the cation is possible for direct ionization from the ground state and can explain the prompt formation of the fragment ion, it does not explain the delayed production of the fragment ion.

While in this study we observe the fragmentation pathway to the hydroxyphenoxy fragment, many previous studies have observed other dissociation channels, which should also be operative in our experiments. However, in order for us to detect them, we need to be able to ionize and observe the formed fragments. We calculated the ionization potentials for both the HONO and hydroxyphenoxy fragments [at the EOM-IP-CCSD/6-311+G(d) level], which are 10.84 and 8.11 eV, respectively, indicating we are not able to measure HONO formation with our probe pulses, while the production of hydroxyphenoxy is just barely observable with threshold ionization by the probe. Therefore, our measurements do not rule out HONO formation, as we are simply not able to observe it if formed.

V. CONCLUDING REMARKS

TRPES and TRIS experiments were performed on o-nitrophenol pumped at 255 nm to the S_4 state. Previous TRPES data of this excited state led to speculation regarding the dynamics from this state, 21 but the combination of TRPES and TRIS more clearly reveal a process of internal conversion followed by intersystem crossing. The ability to distinguish between different

ions and to measure separately their time-dependent yields led to evidence of a novel reaction mechanism resulting in dissociation to form hydroxyphenoxy and NO. The experimental results are found to agree with electronic structure calculations and LIICs for the proposed dissociation mechanism. In particular, the LIICs show a much smaller energy barrier on the T₁ state compared to S₁, greatly strengthening the evidence of intersystem crossing. Altogether, the results illustrate the power of studying quantum molecular dynamics through a combination of multiple observables, with both experiment and theory playing key roles.

ACKNOWLEDGMENTS

The authors gratefully acknowledge support from the National Science Foundation under Award No. 2102319 and helpful discussions with Thomas Allison, Benjamin Levine, and Myles Sylfies.

AUTHOR DECLARATIONS

Conflict of Interest

The authors have no conflicts to disclose.

Author Contributions

Samuel McClung: Conceptualization (supporting); Data curation (lead); Formal analysis (lead); Investigation (lead); Methodology (equal); Resources (supporting); Software (lead); Validation (equal); Visualization (lead); Writing - original draft (lead); Writing review & editing (equal). Dakshitha Abeygunewardane: Conceptualization (supporting); Data curation (lead); Formal analysis (lead); Investigation (lead); Methodology (equal); Software (lead); Validation (equal); Visualization (lead); Writing - original draft (supporting); Writing - review & editing (equal). Spiridoula Matsika: Conceptualization (lead); Data curation (supporting); Formal analysis (supporting); Funding acquisition (lead); Investigation (supporting); Methodology (equal); Project administration (lead); Resources (lead); Software (supporting); Supervision (lead); Validation (equal); Writing - original draft (supporting); Writing - review & editing (equal). Thomas Weinacht: Conceptualization (lead); Data curation (supporting); Formal analysis (supporting); Funding acquisition (lead); Investigation (supporting); Methodology (equal); Project administration (lead); Resources (lead); Software (supporting); Supervision (lead); Validation (equal); Writing - original draft (supporting); Writing – review & editing (equal).

DATA AVAILABILITY

The data that support the findings of this study are available from the corresponding author upon reasonable request.

APPENDIX A: FURTHER REMARKS ABOUT THE HYDROXYPHENOXY YIELD FIT

Before the current fit model was developed, a simpler model was tested in which the parent ion yield follows an exponential decay

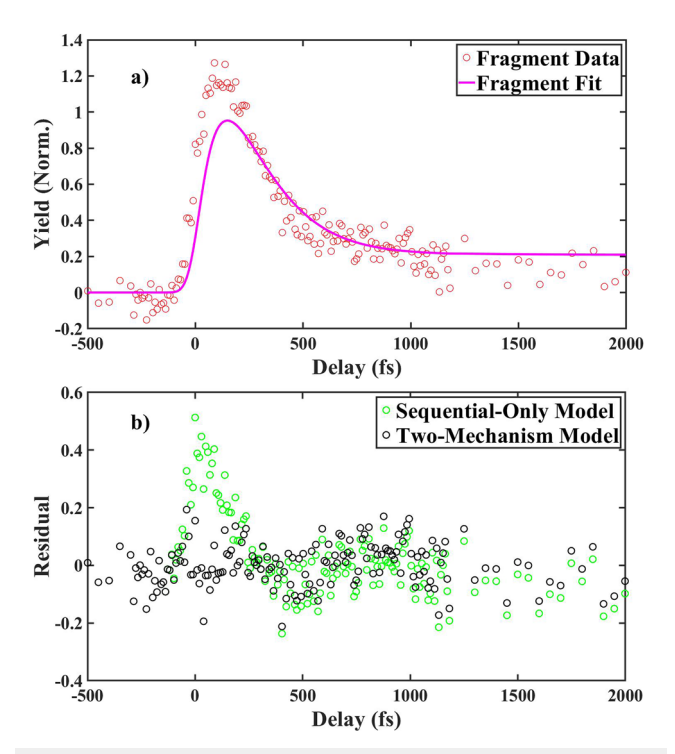


FIG. 6. (a) Hydroxyphenoxy yield, together with the simple model assuming only a sequential decay pathway. (b) Residuals for the simple model (green) and the model used in the main text (black).

as noted previously and the hydroxyphenoxy fragment yield follows only the sequential mechanism such that

$$N_{fragment}(t) = \theta(t_0) \left(\frac{\tau_2}{\tau_1 - \tau_2} N_{parent}(t_0) \left(e^{-(t - t_0)/\tau_1} - e^{-(t - t_0)/\tau_2} \right) + C \right)$$
(A1)

as $N_{fragment}(t_0)=0$ in this case. However, as shown in Fig. 6, despite optimization this model still failed to capture the dynamics of hydroxyphenoxy yield near time zero, where the fit curve rises too late and does not reach the amplitude of the data. These results motivated the more complex model described previously. Further comparison of the two fitting models is shown in the residuals calculated for both fits, in the second plot of Fig. 6. The deviations from zero in the residuals for the "sequential-only" fit parallel the inaccuracies of the fit near time zero.

As noted in the main text, we calculated the energies of the ionic states between the neutral ground state and the Spiro intermediate in order to determine whether the hydroxyphenoxy yield could be explained by dissociation of the cation after ionization by the probe pulse. Figure 7 shows the energies of the first few neutral and ionic states as a function of the C–O bond length associated with the Spiro intermediate.

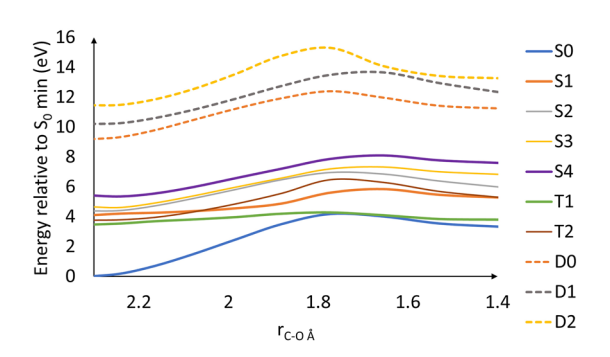


FIG. 7. Energies for the relevant neutral (using EOM-EE-CCSD) and ionic (using EOM-IP-CCSD) states as a function of C-O bond length. The ionic states and neutral singlet states all display a barrier to dissociation, while the lowest lying triplet has no barrier. The energies are only calculated up to the Spiro intermediate since the CCSD cannot properly describe the subsequent dissociation.

APPENDIX B: DERIVATION OF THE FITTING **EQUATION FOR THE HYDROXYPHENOXY ION YIELD**

As described in the main text, the hydroxyphenoxy ion fit has two components, given by the equations

$$N_{fragment,1}(t) = N_{fragment}(t_0)e^{-(t-t_0)/\tau_2},$$
 (B1)

$$N_{fragment,2}(t) = N_{fragment}(t_0)e^{-(t-t_0)/\tau_2} + \frac{\tau_2}{\tau_1 - \tau_2}N_{parent}(t_0)(e^{-(t-t_0)/\tau_1} - e^{-(t-t_0)/\tau_2}).$$
(B2)

The first equation models a simple exponential decay from an initial amplitude. The second equation, derived below, follows a sequential model in which the rise in the hydroxyphenoxy ion yield occurs as a result of the decay in the parent ion yield. In accordance, the derivation of the equation for $N_{fragment,2}(t)$ begins with the differential equation

$$\frac{dN_{fragment,2}(t)}{dt} = \frac{N_{parent}(t)}{\tau_1} - \frac{N_{fragment,2}(t)}{\tau_2}.$$
 (B3)

Substituting the exponential solution for the parent ion yield, this equation becomes

$$\frac{dN_{fragment,2}(t)}{dt} = \frac{N_{parent}(t_0)e^{-(t-t_0)/\tau_1}}{\tau_1} - \frac{N_{fragment,2}(t)}{\tau_2}.$$
 (B4)

Multiplication of the terms by e^{t/τ_2} , along with some simple rearrangement, leads to the result

$$e^{t/\tau_{2}} \frac{dN_{fragment,2}(t)}{dt} + e^{t/\tau_{2}} \frac{N_{fragment,2}(t)}{\tau_{2}} = e^{t/\tau_{2}} \frac{N_{parent}(t_{0})e^{-(t-t_{0})/\tau_{1}}}{\tau_{1}}.$$
(B5)

However, the left side of the equation can be represented as a single derivative,

$$\frac{d}{dt}(e^{t/\tau_2}N_{fragment,2}(t)) = e^{t/\tau_2} \frac{N_{parent}(t_0)e^{-(t-t_0)/\tau_1}}{\tau_1}.$$
 (B6)

Integration leads to the result

$$e^{t/\tau_2} N_{fragment,2}(t) = \frac{\tau_2}{\tau_1 - \tau_2} N_{parent}(t_0) e^{t_0/\tau_1} e^{(1/\tau_2 - 1/\tau_1)t} + K,$$
 (B7)

in which K is a constant. The initial condition at $t = t_0$ is used to solve for *K*,

$$K = N_{fragment}(t_0)e^{t_0/\tau_2} - \frac{\tau_2}{\tau_1 - \tau_2}N_{parent}(t_0)e^{t_0/\tau_2}.$$
 (B8)

Substituting this value for *K*, the integrated equation becomes

$$e^{t/\tau_{2}}N_{fragment,2}(t) = \frac{\tau_{2}}{\tau_{1} - \tau_{2}}N_{parent}(t_{0})e^{t_{0}/\tau_{1}}e^{(1/\tau_{2} - 1/\tau_{1})t} + N_{fragment}(t_{0})e^{t_{0}/\tau_{2}} - \frac{\tau_{2}}{\tau_{1} - \tau_{2}}N_{parent}(t_{0})e^{t_{0}/\tau_{2}}.$$
 (B9)

Finally, division by e^{t/τ_2} on both sides of the equation and rearrangement of terms give the equation for the fragment ion yield as a function of time,

$$N_{fragment,2}(t) = \frac{\tau_2}{\tau_1 - \tau_2} N_{parent}(t_0) \left(e^{-(t-t_0)/\tau_1} - e^{-(t-t_0)/\tau_2} \right) + N_{fragment}(t_0) e^{-(t-t_0)/\tau_2}.$$
 (B10)

As described in the main text, the full hydroxyphenoxy yield is modeled as a superposition of the two components,

$$N_{fragment}(t) = \alpha N_{fragment,1}(t) + \beta N_{fragment,2}(t) + C,$$
 (B11)

in which $\alpha + \beta = 1$. Substituting the equations for $N_{fragment,1}(t)$ and $N_{fragment,2}$,

$$N_{fragment}(t) = \alpha N_{fragment}(t_0) e^{-(t-t_0)/\tau_2}$$

$$+ \beta N_{fragment}(t_0) e^{-(t-t_0)/\tau_2} + \frac{\beta \tau_2}{\tau_1 - \tau_2} N_{parent}(t_0)$$

$$\times (e^{-(t-t_0)/\tau_1} - e^{-(t-t_0)/\tau_2}) + C.$$
(B12)

However, because $\alpha + \beta = 1$, the equation simplifies to

$$N_{fragment}(t) = N_{fragment}(t_0)e^{-(t-t_0)/\tau_2} + \frac{\beta \tau_2}{\tau_1 - \tau_2} N_{parent}(t_0) \times (e^{-(t-t_0)/\tau_1} - e^{-(t-t_0)/\tau_2}) + C,$$
(B13)

leading to the final form of the fitting equation for the hydroxyphenoxy yield.

APPENDIX C: COMPARISON OF INTEGRATED TRPES ENERGIES TO ION YIELDS

For a closer comparison between ion and electron data, the TRPES spectrum shown in Fig. 3 was integrated along different energy "bands" at each delay, as shown in Fig. 8. The first panel in the figure shows that the high-energy electrons (1.5-4.0 eV) roughly track the parent ion, while the low-energy electrons (0-1.5 eV) roughly track the fragment ion. As shown in the second panel, focusing in on a narrower region at the lowest energies (0-0.8 eV) shows

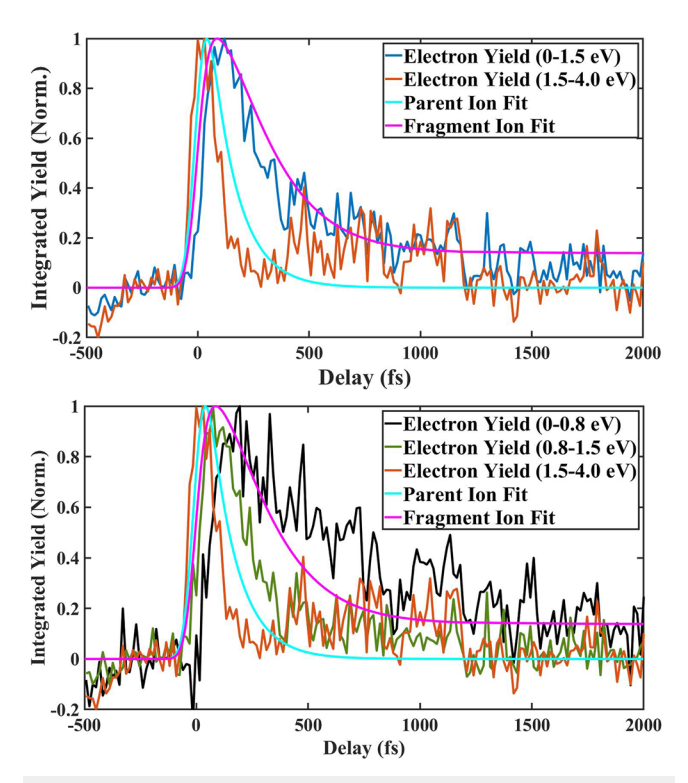


FIG. 8. Ion yields in comparison with integrated energy "bands" of the TRPES spectrum for each delay. All ion and integrated electron yields are scaled individually such that the maximum yield of each ion fit or electron integration region is one.

a clearer parallel with the fragment ion yield at long times. In this figure, all ion and integrated electron yields are scaled individually such that the maximum yield of each ion fit or electron data integration is one. While it is tempting to associate the highest energy electrons with geometries close to the FC point, middle energy electrons with the Spiro intermediate, and the lowest energy electrons with the formation of hydroxyphenoxy, this is likely a gross oversimplification. For this reason, it is more scrupulous to associate the decay of the photoelectron energy only loosely with the general progression from the FC geometry through the Spiro intermediate to the hydroxyphenoxy product.

REFERENCES

¹Y.-C. Cheng and G. R. Fleming, "Dynamics of light harvesting in photosynthesis," Annu. Rev. Phys. Chem. **60**, 241–262 (2009).

²C. Canuel, M. Mons, F. Piuzzi, B. Tardivel, I. Dimicoli, and M. Elhanine, "Excited states dynamics of DNA and RNA bases: Characterization of a stepwise deactivation pathway in the gas phase," J. Chem. Phys. 122, 074316 (2005).

³T. Gustavsson, R. Improta, and D. Markovitsi, "DNA/RNA: Building blocks of life under UV irradiation," J. Phys. Chem. Lett. 1, 2025–2030 (2010).

⁴J.-M. L. Pecourt, J. Peon, and B. Kohler, "Ultrafast internal conversion of electronically excited RNA and DNA nucleosides in water," J. Am. Chem. Soc. 122, 9348–9349 (2000).

⁵I. McConnell, G. Li, and G. W. Brudvig, "Energy conversion in natural and artificial photosynthesis," Chem. Biol. 17, 434–447 (2010).

⁶C. Jin, E. Y. Ma, O. Karni, E. C. Regan, F. Wang, and T. F. Heinz, "Ultrafast dynamics in van der Waals heterostructures," Nat. Nanotechnol. **13**, 994–1003 (2018).

⁷A. Stolow, A. E. Bragg, and D. M. Neumark, "Femtosecond time-resolved photoelectron spectroscopy," Chem. Rev. **104**, 1719–1758 (2004).

⁸S. P. Weathersby, G. Brown, M. Centurion, T. F. Chase, R. Coffee, J. Corbett, J. P. Eichner, J. C. Frisch, A. R. Fry, M. Gühr *et al.*, "Mega-electron-volt ultrafast electron diffraction at SLAC national accelerator laboratory," Rev. Sci. Instrum. **86**, 073702 (2015).

⁹J. Yang, X. Zhu, J. P. F. Nunes, J. K. Yu, R. M. Parrish, T. J. A. Wolf, M. Centurion, M. Gühr, R. Li, Y. Liu *et al.*, "Simultaneous observation of nuclear and electronic dynamics by ultrafast electron diffraction," Science 368, 885–889 (2020).

¹⁶Y. Liu, S. L. Horton, J. Yang, J. P. F. Nunes, X. Shen, T. J. Wolf, R. Forbes, C. Cheng, B. Moore, M. Centurion *et al.*, "Spectroscopic and structural probing of excited-state molecular dynamics with time-resolved photoelectron spectroscopy and ultrafast electron diffraction," Phys. Rev. X 10, 021016 (2020).

¹¹B. Stankus, H. Yong, N. Zotev, J. M. Ruddock, D. Bellshaw, T. J. Lane, M. Liang, S. Boutet, S. Carbajo, J. S. Robinson *et al.*, "Ultrafast X-ray scattering reveals vibrational coherence following Rydberg excitation," Nat. Chem. **11**, 716–721 (2019).

¹²Y. Liu, T. Rozgonyi, P. Marquetand, and T. Weinacht, "Excited-state dynamics of CH₂I₂ and CH₂IBR studied with UV-pump VUV-probe momentum-resolved photoion spectroscopy," J. Chem. Phys. 153, 184304 (2020).

¹³I. Bejan, Y. Abd El Aal, I. Barnes, T. Benter, B. Bohn, P. Wiesen, and J. Kleffmann, "The photolysis of *ortho*-nitrophenols: A new gas phase source of HONO," Phys. Chem. Chem. Phys. 8, 2028–2035 (2006).

¹⁴Y.-Q. Wang, H.-G. Wang, S.-Q. Zhang, K.-M. Pei, X. Zheng, and D. Lee Phillips, "Resonance Raman intensity analysis of the excited state proton transfer dynamics of 2-nitrophenol in the charge-transfer band absorption," J. Chem. Phys. 125, 214506 (2006).

¹⁵H. A. Ernst, T. J. A. Wolf, O. Schalk, N. González-García, A. E. Boguslavskiy, A. Stolow, M. Olzmann, and A.-N. Unterreiner, "Ultrafast dynamics of o-nitrophenol: An experimental and theoretical study," J. Phys. Chem. A 119, 9225–9235 (2015).

¹⁶Y. Nitta, O. Schalk, H. Igarashi, S. Wada, T. Tsutsumi, K. Saita, T. Taketsugu, and T. Sekikawa, "Real-time probing of an atmospheric photochemical reaction by ultrashort extreme ultraviolet pulses: Nitrous acid release from *o*-nitrophenol," J. Phys. Chem. Lett. **12**, 674–679 (2021).

¹⁷C. Xu, L. Yu, C. Zhu, and J. Yu, "Photoisomerization reaction mechanisms of *o*-nitrophenol revealed by analyzing intersystem crossing network at the MRCI level," J. Phys. Chem. A **119**, 10441–10450 (2015).

¹⁸C. Xu, L. Yu, C. Zhu, J. Yu, and Z. Cao, "Intersystem crossing-branched excited-state intramolecular proton transfer for o-nitrophenol: An ab initio on-the-fly nonadiabatic molecular dynamic simulation," Sci. Rep. 6, 26768 (2016).

¹⁹C. Xu, F. L. Gu, and C. Zhu, "Ultrafast intersystem crossing for nitrophenols: *Ab initio* nonadiabatic molecular dynamics simulation," Phys. Chem. Chem. Phys. **20**, 5606–5616 (2018).

²⁰L. Vereecken, H. K. Chakravarty, B. Bohn, and J. Lelieveld, "Theoretical study on the formation of H- and O-atoms, HONO, OH, NO, and NO₂ from the lowest lying singlet and triplet states in *ortho*-nitrophenol photolysis," Int. J. Chem. Kinet. 48, 785–795 (2016).

²¹ A. Ciavardini, M. Coreno, C. Callegari, C. Spezzani, G. De Ninno, B. Ressel, C. Grazioli, M. de Simone, A. Kivimäki, P. Miotti *et al.*, "Ultra-fast-VUV photoemission study of UV excited 2-nitrophenol," J. Phys. Chem. A **123**, 1295–1302 (2019).

²² M. Beutler, M. Ghotbi, F. Noack, and I. V. Hertel, "Generation of sub-50-fs vacuum ultraviolet pulses by four-wave mixing in argon," Opt. Lett. 35, 1491–1493 (2010).

²³P. Farmanara, O. Steinkellner, M. T. Wick, M. Wittmann, G. Korn, V. Stert, and W. Radloff, "Ultrafast internal conversion and photodissociation of molecules excited by femtosecond 155 nm laser pulses," J. Chem. Phys. 111, 6264–6270 (1999)

²⁴T. K. Allison III, "Femtosecond molecular dynamics studied with vacuum ultraviolet pulse pairs," Ph.D. thesis, University of California, Berkeley, 2010.

 ²⁵Y. Liu, "Combining spectroscopic and structural probes of molecular dynamics," Ph.D. thesis, Stony Brook University, 2021.
 ²⁶NIST Mass Spectrometry Data Center, "Mass spectra," in NIST Chemistry Web-Book, NIST Standard Reference Database Number 69, edited by P. Linstrom and W. Mallard (National Institute of Standards and Technology, 2014).

 $^{^{\}bf 27}$ S. L. Horton, "Photoionizaion as a probe of ultrafast molecular dynamics," Ph.D. thesis, Stony Brook University, 2018.

²⁸M. Assmann, T. Weinacht, and S. Matsika, "Surface hopping investigation of the relaxation dynamics in radical cations," J. Chem. Phys. 144, 034301